

1 **Elemental Stoichiometry of Particulate Organic Matter across the Atlantic Ocean**

2
3 Adam J. Fagan¹, Tatsuro Tanioka¹, Alyse A. Larkin¹, Jenna A. Lee¹, Nathan S. Garcia¹, & Adam
4 C. Martiny^{1,2,*}

5 ¹Department of Earth System Science, University of California, Irvine, CA, USA

6
7 ²Department of Ecology and Evolutionary Biology, University of California, Irvine, CA, USA

8 *Corresponding Author: amartiny@uci.edu

9
10 **Abstract:**

11 Recent studies show that stoichiometric elemental ratios of marine ecosystems are not static at
12 Redfield proportions but vary systematically between biomes. However, the wider Atlantic
13 Ocean is under-sampled for particulate organic matter (POM) elemental composition, especially
14 as it comes to phosphorus (i.e., POP). Thus, it is uncertain how environmental variation in this
15 region translates into shifts in C:N:P. To address this, we analyzed hydrography, genomics, and
16 POM concentrations from 877 stations on the meridional transects AMT28 and C13.5, spanning
17 the Atlantic Ocean. We observed nutrient-replete, high-latitude ecosystem C:N:P to be
18 significantly lower than the oligotrophic gyres. Latitudinal and zonal differences in elemental
19 stoichiometry were linked to overall nutrient supply as well as N vs. P stress. C:P and N:P were
20 generally higher in the P-stressed northern region compared to southern hemisphere regions. We
21 also detected a zonal difference linked to a westward deepening nutricline and a shift from N to
22 P stress. We also evaluated possible seasonal changes in C:N:P across the basin and predicted
23 these to be limited. Overall, this study confirms latitudinal shifts in surface ocean POM ratios but
24 reveals previously unrecognized hemisphere and zonal gradients. This work demonstrates the
25 importance of understanding how regional shifts in hydrography and type of nutrient stress shape
26 the coupling between Atlantic Ocean nutrient and carbon cycles.

29 **Plain language summary:**

30 Climate change is predicted to influence the biological pump by altering phytoplankton nutrient
31 distribution. In our research, we conducted comprehensive measurements of particulate matter
32 concentrations during two large oceanographic field studies. We observed systematic variations
33 in organic matter concentrations and ratios across the Atlantic Ocean, both latitudinally and
34 longitudinally. Through statistical modeling, we determined that these variations are associated
35 with differences in the availability of essential nutrients for phytoplankton growth. Our findings
36 highlight the adaptive resource utilization among surface ocean plankton, which in turn
37 modulates the interplay between the ocean's nutrient and carbon cycles.

38

39 **Key points:**

- 40 • There was systematic regional variation in POM concentrations and ratios across the
41 Atlantic Ocean.
- 42 • Latitudinal variability in C:N:P is linked to the nutrient supply rate and N vs. P stress.
- 43 • Westward deepening isopycnals and nutricline and a shift from N to P stress correspond
44 to zonal variability in C:N:P

45

46
47
48
49
50
51
52
53
54
55
56
57
58
59
60
61
62
63
64
65
66
67
68
69
70
71
72
73
74
75
76
77
78
79
80
81
82
83
84
85
86
87
88
89
90
91

1. Introduction

The efficiency of the biological pump is anticipated to be affected by climate change through alteration in phytoplankton nutrient allocation and the C:N:P ratio (Galbraith + Martiny, 2015). Nevertheless, the influence of ocean warming on this efficiency is still uncertain, carrying potential repercussions for the ecosystems and global carbon cycle (Kwon et al., 2022). Over the past few decades, studies have observed variability in marine plankton elemental composition and ecosystem elemental composition (Weber and Deutsch, 2010; Martiny et al., 2013b, a). Specifically, regions with nutrient-rich conditions have lower C:N:P ratios (equatorial, coastal, and temperate regions), and nutrient-poor conditions (subtropical gyre regions) have higher ratios (Martiny et al., 2013b, a). However, data compilations include variations in both sampling and analytical methodologies (Martiny et al., 2014) as well as have limited spatial coverage. Therefore, large-scale sampling efforts like Bio-GO-SHIP are quantifying ecosystem particulate organic matter (POM) concentrations and their elemental ratios utilizing consistent methodologies on a global scale (Tanioka et al., 2022; Clayton et al., 2022).

Studies focused on POM stoichiometry across ocean basins have been primarily limited to Bio-GO-SHIP cruises within the Indian Ocean (Garcia et al., 2018) and the Pacific Ocean (Lee et al., 2021). Both studies have observed high POM concentrations at higher latitudes and low concentrations within the gyres, with intermediate levels toward the equator. The stoichiometry had higher values in the gyres and lower values at high latitudes (Garcia et al., 2018; Lee et al., 2021). There have been two basins-wide transects across the Atlantic ocean that have been used in a global synthesis (Tanioka et al., 2022) but have not been used in a study focused solely on the Atlantic. Along with the strong relationship with latitude, there is also strong correlation with nutricline depth, used as a proxy for nutrient flux, in the global synthesis. Localized studies at the Bermuda Atlantic Time-series (BATS) site or short transects along the western North Atlantic Ocean show an N:P ratio between 40–50 and C:N near Redfield proportions (~6.6) (Michaels et al., 1994; Michaels and Knap, 1996; Steinberg et al., 2001; Babiker et al., 2004; Cavender-Bares et al., 2001). In contrast, POM dynamics and especially N:P and C:P ratios are less understood within the NE Atlantic Ocean and South Atlantic Ocean as a whole.

The Atlantic Ocean has a unique dynamic, being singularly/ co-limited by nitrogen and phosphorus respectively to the north of the equator and predominantly nitrogen limited south of the equator (Cotner et al., 1997; Mather et al., 2008; Browning and Moore, 2023). In phosphorus co-limited regions, N:P and C:P are often elevated from frugal phosphorus use, supported by the well sampled NW Atlantic Ocean (Galbraith and Martiny, 2015; Lomas et al., 2010, 2022). As a response to the nutrient limitation, phytoplankton can express specific genes that will allow for greater uptake of a nutrient. Gene expression and preferential uptake could influence cellular C:N:P within phytoplankton. Nitrogen limitation is more widespread in the South Atlantic Ocean, but no study has quantified ecosystem C:N:P here (Mather et al., 2008; Ustick et al., 2021). Temperature has been known to influence the concentration of cellular phosphorus in phytoplankton, with increasing in C:P with warmer temperatures, however C:N remains unchanged (Yvon-Durocher et al., 2015). The underlying mechanism for this relationship is not fully understood but hypothesized to be from either increase in carbon uptake over phosphorus, an increase in nutrient use efficiency, or translation compensation theory (few P-rich ribosomes are required for protein synthesis) (Tanioka and Matsumoto, 2020). The availability of nutrients

92 generally follow inverse patterns of C:N:P, with increasing nutrients leading to a decrease in C:N
93 and C:P and vice-versa (Galbraith and Martiny, 2015; Tanioka and Matsumoto, 2017). However,
94 such environmental variation in the Atlantic Ocean elemental stoichiometry remains largely
95 unknown. Therefore, the broad environmental gradients in the Atlantic Ocean could result in
96 significant regional ecosystem C:N:P shifts.

97 Here, we quantified suspended particulate organic carbon, nitrogen, and phosphorus
98 concentrations along two Bio-GO-SHIP meridional transects: AMT 28 and C13.5 (Fig. 1),
99 covering large parts of the Atlantic Ocean. We addressed two questions: (1) What are
100 meridional, hemispheric, and zonal differences in POM concentrations and stoichiometry? And
101 (2) What is the relationship between environmental factors and C:N:P? We hypothesize that
102 differences in total nutrient supply and temperature are primarily responsible for the latitudinal
103 gradient in C:N:P. In contrast, the type of nutrient stress will be important for hemispheric and
104 longitudinal C:N:P shifts.

105

106 **2. Methods**

107 **2.1. Cruise Transects**

108

109 AMT 28 started in Harwich, UK (49° 38' N/5° 30' W), and ended in Mare Harbour, Falkland
110 Islands (48° 12' S/52° 42' W), departing the 25 September 2018, and ending the 27 October
111 2018. C13.5 started in Cape Town, South Africa (34° 22' S/17° 18' W), and ended in Norfolk,
112 VA (36° 5' N/74° 34' W) (Fig. 1), departing the 21 March 2020, and ending the 16 April 2020.
113 C13.5 was set to go 45° S and collect samples along the eastern boundary of the South Atlantic
114 Ocean. Due to COVID-19 quarantine restrictions, it was redirected to a port in Virginia.
115 Fortuitously, this redirect allowed sample collection across the eastern South Atlantic Ocean and
116 the western North Atlantic Ocean.

117

118 **2.2. Sample collection**

119

120 Seawater for the POM was collected from the underway flow-through system for both cruises at
121 a depth of approximately 5 m. This method involved initially passing water through a 30 µm
122 nylon mesh to remove the stochastic presence of large particles from the samples (Lee et al.,
123 2021). We then collected 3 to 8 L of filtered water in 8.5 L plastic polycarbonate carboys
124 (Thermo Fisher Scientific, Waltham, MA). The carboys were placed at a 45° angle to prevent
125 particles from settling below the nozzle. Next, particulate organic carbon (POC)/ nitrogen
126 (PON), and phosphorus (POP) samples were filtered onto 25 mm pre-combusted GF/F (500° C
127 for 5 hours)(nominal pore size of 0.7 µm) (Whatman, Florham Park, NJ) (POC/PON are on the
128 same filter). POP filters were rinsed with 5 ml of 0.17 M Na₂SO₄ to remove traces of dissolved
129 phosphorous from the filter. Finally, we stored all filters in pre-combusted aluminum packets and
130 placed them in a -80° C freezer during the cruise, a -20° C cooler for shipping, and back to a
131 -80° C freezer until analysis. Between sample collections, the carboys and tubing were rinsed
132 with 30 µm filtered sample water just prior to collection.

133 We collected single samples of POC/PON and POP hourly for AMT 28. For the C13.5
134 transect, POC/PON and POP samples were collected in triplicate every 4 to 6 hours. Water
135 collection for C13.5 was done at the peak and trough of the diel cycle, ~06:00 and ~20:00 LT,
136 respectively, and with one to two collections in between those times.

137

138 **2.3. Particulate organic matter determination**

139 2.3.1. Particulate organic phosphorus (POP) assay

140
141 POP was analyzed using a modified ash-hydrolysis protocol (Lomas et al., 2010). Filters were
142 placed into acid-washed/pre-combusted glass vials with 2 ml of 0.017 M MgSO₄ and covered
143 with pre-combusted aluminum foil. The vials were placed in an incubator for 24 hours at 80 to
144 90° C and then combusted for 2 hours at 500° C. After cooling, 5 ml of 0.2 M HCl was added
145 and incubated at 80 to 90° C for 30 minutes. The supernatant was collected, and the vials were
146 rinsed with 5 ml of Milli-Q water. The rinse water was collected and added to the supernatant. 1
147 ml of mixed reagent (2:5:1:2 parts ammonium molybdate tetrahydrate (24.3 mM), sulfuric acid
148 (5 N), potassium antimonyl tartrate (4.1 mM), and ascorbic acid (0.3 M) was added to the
149 supernatant and left in the dark for 30 minutes. Samples were analyzed on a spectrophotometer at
150 a wavelength of 885 nm using a potassium monobasic phosphate standard (1.0 mM-P). The
151 detection limit for POP measurements was ~0.3 µg.

152

153 2.3.2. Particulate organic carbon/nitrogen (POC/PON) assay

154
155 POC/PON are measured using the same filter. The POC/PON samples were processed in the lab
156 at UCI using a JGOFS protocol (Ducklow and Dickson, 1994). POC/PON samples were dried in
157 an incubator at 55° C for 24 hours. They were then moved to a desiccator with concentrated HCl
158 fumes for 24 hours to remove inorganic carbon. The samples were then re-dried at 55° C for 24
159 hours before being packaged into pre-combusted tin capsules (CE Elantech, Lakewood, NJ). The
160 packaged filters were analyzed on a CN FlashEA 1112 Elemental Analyzer (Thermo Scientific,
161 Waltham, MA) with atropine and acetanilide standards. POC and PON measurements had a
162 detection limit of ~2.4 µg and ~3.0 µg. Settings for the FlashEA had an oxidative reactor
163 temperature of 900° C, a reduction reactor temperature of 680° C, and an oven temperature of
164 50° C. Oxygen introduced to the oxidative reactor last seven seconds allowing temperatures to
165 reach 1800° C for sample combustion. A leak test needed to fall below 5 ml min⁻¹ before
166 samples were analyzed to minimize sample loss.

167

168 2.4. Nutrient availability, biogeography, and biological properties

169 2.4.1. Nutricline depth

170

171 The nutricline depth was determined as the 1 µM nitrate depth horizon (Garcia et al., 2018;
172 Cermeño et al., 2008). Nutricline depth was regarded as a proxy for nutrient supply to the
173 surface, with a shallow nutricline representing a high flux of nutrients and vice versa for a deep
174 nutricline. The nutricline depth with respect to the 1/16 µM phosphate depth horizon was also
175 investigated but found to be nearly identical to that of nitrate. For AMT28, nitrate concentrations
176 were quantified as previously described from CTD casts along the transect (Swift, 2019). Nitrate
177 concentrations were then interpolated using DIVA implemented in Ocean Data View (v5.5.2)
178 (Schlitzer, 2019). For C13.5, we used the seasonal average nitrate depth profiles from 2018 of
179 the World Ocean Atlas at one degree spatial resolution to determine nutricline depths. This
180 approach was necessary as the logistical issues related to COVID quarantine restrictions
181 prevented us from collecting onboard CTD measurements. Linear interpolation for each profile
182 within the one degree was performed to estimate the nutricline depth.

183

184 2.4.2. Delineation of Regions

185
186 The regions under consideration for this study are the Eastern Temperate North Atlantic (ETNA)
187 [Lat. 49.6°N-43.2°N] Western North Atlantic Gyre (WNAG) [Lat. 34.5°N-19.8°N], Eastern
188 North Atlantic Gyre (ENAG) [Lat. 43.0°N-18.1°N], Western Equatorial (WEQ) [Lat. 17.9°N-
189 5.9°S], Eastern Equatorial (EEQ) [Lat. 17.8°N-5.9°S], Western South Atlantic Gyre (WSAG)
190 [Lat. 6.0°S-34.0°S], Eastern South Atlantic Gyre (ESAG) [Lat. 6.2°S-33.0°S], Western
191 Temperate South Atlantic (WTSA) [Lat. 34.1°S-48.2°S], and Eastern Temperate South Atlantic
192 (ETSA) [Lat. 33.9°S-41.5°S] (Fig. 1). These boundaries are determined using inflection points
193 along the nutricline depth and the temperature profile.

194 195 2.4.3. Cell size

196
197 Cell size was determined by the conversion of cell count, collected during CTD casts (AMT28)
198 at the top 200 m of the water column. Flow cytometry samples (63 stations, 755 samples) were
199 co-collected with the POM samples used in this study. Cell count was determined using two
200 methodologies. The first method was collected without a filter and utilized an inverted
201 microscope to estimate cell abundance and phytoplankton species composition (Utermöhl, 1958).
202 This allowed for the estimates of diatoms, dinoflagellates, and coccolithophores. The second
203 method measured cells using a Becton Dickinson FACSort flow cytometer to measure
204 *Prochlorococcus*, *Synechococcus*, and pico-eukaryotes. Combining these two methods of
205 collection allowed for a complete survey of phytoplankton groups.

206 Conversion of cell count to biomass (fg C cell) was done following the methodology
207 from Moreno et al., 2022. Photoautotrophs were categorized into *Prochlorococcus*,
208 *Synechococcus*, pico-eukaryotes, nano-eukaryotes, *Coccolithophore*, and *Cryptophytes*. Each cell
209 type had a specific conversion factor in determining its biomass. Using a Monte Carlo approach,
210 95% confidence interval around cell size was determined using a normal distribution based on
211 the mean and standard deviation. Then, a randomly chosen conversion factor was applied to each
212 type. Allowing for 1000 runs, we estimate a 95% confidence interval (Moreno et al., 2022).

213 214 2.4.4. Metagenomics-informed nutrient stress

215
216 Metagenomically informed nutrient stress utilizes a subset of data from Ustick et al., 2021,
217 utilizing the genome content of *Prochlorococcus* from the Atlantic Ocean. These metagenomic
218 samples (276) were co-collected with the POM samples, across both transects, used in this study.
219 Based on variation in *Prochlorococcus* population gene content, this study identified genes
220 associated with nitrogen and phosphorus nutrient stress types. The severity of nutrient stress was
221 quantified by calculating the frequency of nutrient acquisition genes within *Prochlorococcus*
222 single-copy core genes and attributes the frequency to the genetic adaptation for overcoming
223 nutrient stress type and severity. Moving forward the use of nitrogen/phosphorus gene index will
224 refer to this calculation of nutrient stress. Although based on *Prochlorococcus*, there is a
225 significant overlap between this genetic index of nutrient stress and both Earth System Models
226 and whole community nutrient addition assays (Ustick et al., 2021).

227 Ustick et al., 2021 associated *Prochlorococcus* gene occurrences with different
228 environmental nutrient stress conditions. They separated the genes by nutrient type (nitrogen,
229 phosphorus, and iron) and nutrient stress severity (low, medium, and high). Our study utilizes the
230 high stress severity for nitrogen and phosphorus. Iron has a more indirect influence on the C:N:P,

231 than nitrogen and phosphorus, which is why it will be omitted from this study. The stress
232 severity associated with medium or low stress either followed the same pattern as the high
233 nutrient stress or had no pattern at all, respectively, which is why this is also omitted. The
234 function of the genes associated with high gene index are *focA*, *moaA-E*, *moeA*, *napA*, *narB*, *nirA*
235 (for nitrogen) and *phoA*, *phoX* (for phosphorus). The functions of these genes are for the
236 assimilation and uptake of nitrite and nitrate, and production of alkaline phosphatase.

237

238 2.4.5 N^* Derivation

239

240 The derivation from Redfield nutrient concentration (N^*) at a depth of 200 m was calculation:

241

$$242 N^*_{200} = [\text{NO}_3]^{-1}_{200} - 16[\text{PO}_4]^{-3}_{200}$$

243

244 A negative/ declining value would be indicative of nitrogen stress, while a positive/ increasing
245 value would indicate phosphorus stress.

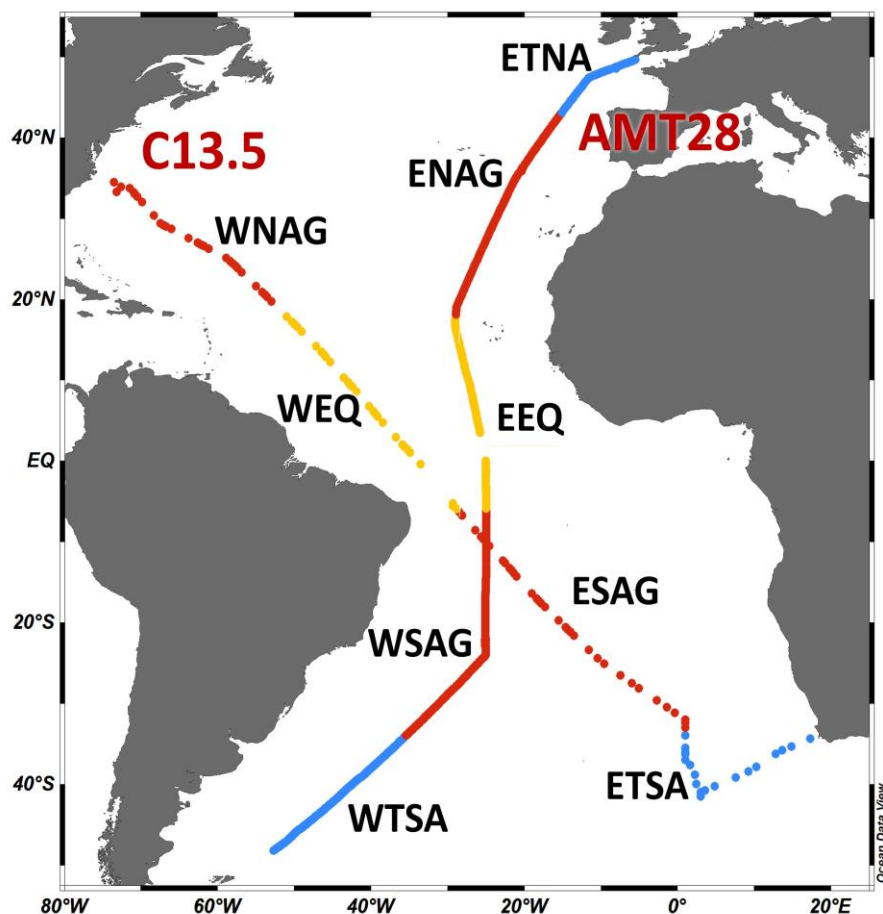
246

247 2.5. Data analysis

248

249 Data analysis was conducted using Matlab R2021b (MathWorks). An ANOVA analysis with a
250 posthoc Tukey test was used to determine the relationship between the selected regions for
251 environmental conditions and POM. The C:N:P ratios underwent a log transformation to achieve
252 a normal distribution before the ANOVA analysis (Isles, 2020). Using R ver. 4.1.2 (R Core
253 Team, 2021), we used generalized additive models (GAM) with package *mgcv* (v1.8) (Wood,
254 2017) to explain the strength of four variables in determining C:N:P (temperature, nutricline
255 depth, nitrogen gene index, and phosphorus gene index).

256

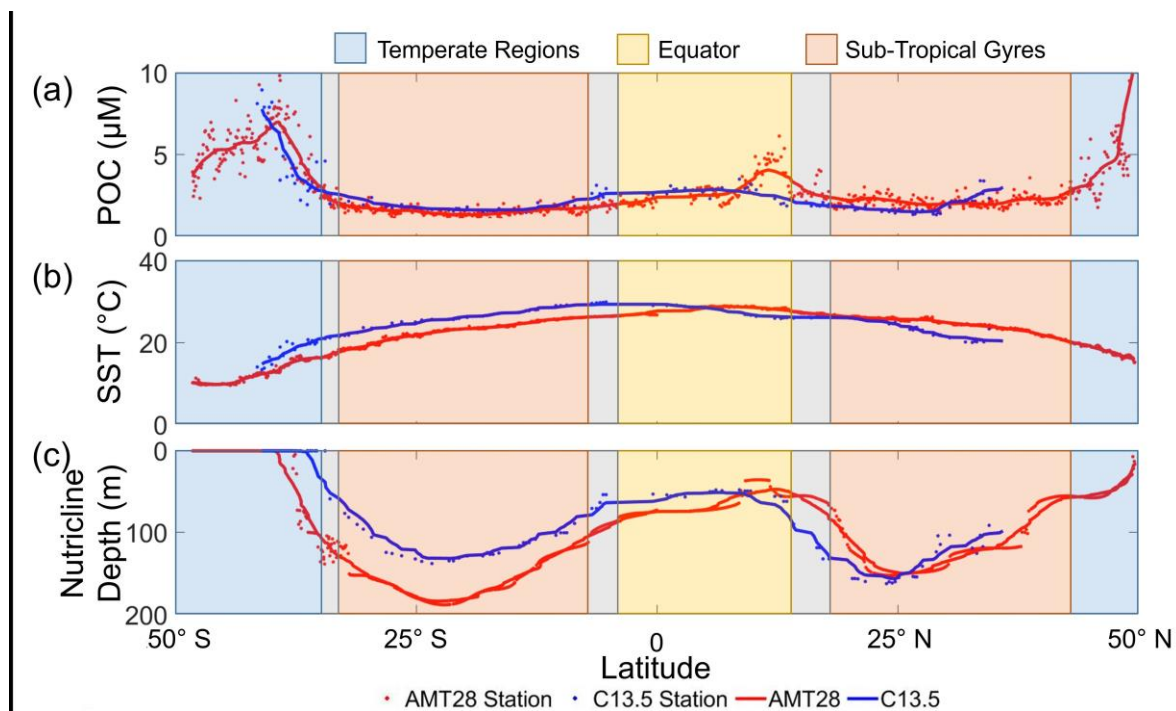


258 **Figure 1.** Map of oceanographic cruise transects AMT 28 (September 25 to October 27, 2018, n = 765)
 259 (March 21 to April 16, 2020, n = 112). Different oceanographic regions are separated using nutricline and
 260 temperature profiles (WTSA = Western Temperate South Atlantic, ETSA = Eastern Temperate South Atlantic,
 261 WSAG = Western South Atlantic Gyre, ESAG = Eastern South Atlantic Gyre, WEQ = Western Equatorial, EEQ =
 262 Eastern Equatorial, WNAG = Western North Atlantic Gyre, ENAG = Eastern North Atlantic Gyre, ETNA = Eastern
 263 Temperate North Atlantic). Colors delineate temperate (blue), subtropical (red), and equatorial upwelling regions
 264 (yellow).
 265
 266

267 POM concentrations, temperature, and nutricline profiles exhibited unique characteristics to each
 268 oceanographic region. Between the two transects, POC, PON, and POP concentrations were
 269 strongly correlated ($r = 0.68, 0.71, \text{ and } 0.70$, respectively; $p < 0.001$) (Fig. 2a and S1). All POM
 270 pools had peak concentrations at high latitudes, troughs in the subtropical gyres, and
 271 intermediate concentrations at the equator. In high latitude temperate regions (WTSA, ETSA,
 272 and ETNA), POC (and overall POM) was significantly elevated ($4.6 \text{ to } 5.3 \mu\text{M}$; $p < 0.05$)
 273 compared to all other regions (Equatorial: $2.8 \mu\text{M}$, Gyre: $1.6 \text{ to } 2.1 \mu\text{M}$) (Fig. 2a, Fig. S2). POM
 274 concentrations also showed a zonal difference. There were higher concentrations of POM in the
 275 western regions compared to the eastern region of the Temperate South Atlantic, whereas the
 276 opposite was seen in the subtropical gyres (Fig. 2a and Fig. S2). At $\sim 10^\circ \text{ S}$, C13.5 and AMT 28
 277 cross paths, we used a 1° cell centered on the intersection (using 9 samples), to find the
 278 difference between the POC, PON, and POP of the two cruises was 0.2%, 5.7%, and 10.6%
 279 respectively, indicating that seasonal variability between the had the greatest impact on POP.
 280 However, one sample is the cause of most of the error, within PON and POP, removing the

281 sample the difference becomes 2.9%, and 2.1% respectively. Temperature peaked equatorially (~
 282 28° C) for both transects and declined with increasing latitudes (Fig. 2b). We observed minor
 283 variation in the meridional temperature profile linked to the difference in the seasonal timing for
 284 each cruise leading to a slight southward shift in peak temperature during C13.5. Nutricline
 285 profiles for both transects were similar, with the deepest nutricline in the gyres and shallowest at
 286 high latitudes and the equator (Fig. 2c). Zonal variability in the nutricline depth was apparent,
 287 with the deepest values in the western side (135 to 150 m) compared to the eastern side of the
 288 gyres (114 to 116 m) (Fig. S2). Thus, we observed a robust meridional gradient in POM
 289 concentrations and environmental conditions but also a zonal gradient in nutricline depth in the
 290 oligotrophic subtropical gyres.

291
 292

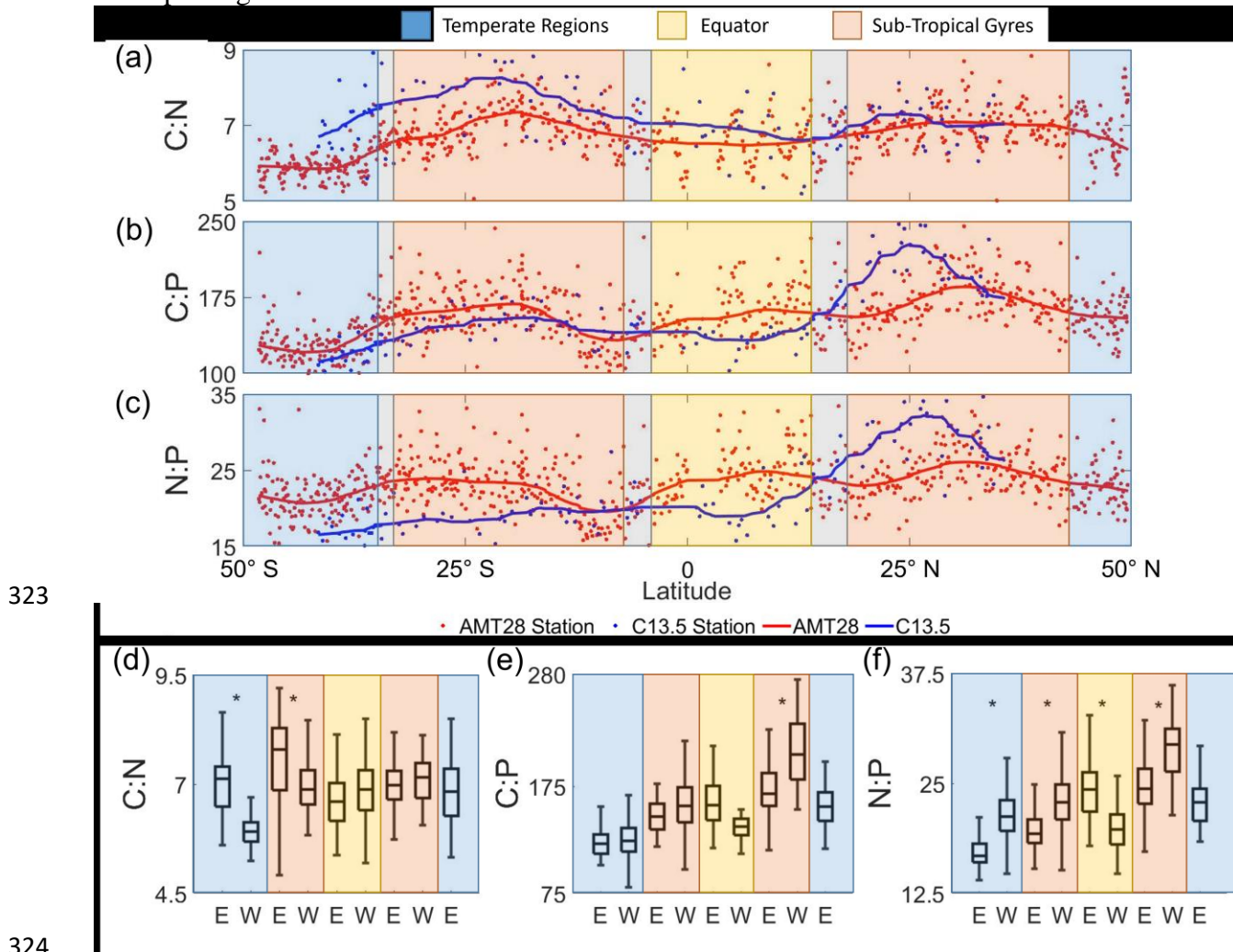


293
 294 **Figure 2.** Meridional variability in POC concentrations and environmental conditions for AMT28 (boreal fall) and
 295 C13.5 (boreal spring). (a) Averaged surface POC concentrations, (b) surface temperature, and (c) nutricline depth
 296 presented as $Z_{\text{nitrate}} > 1 \mu\text{M}$. The trend lines represent the moving average of samples for AMT28 (red/ n=50) and
 297 C13.5 (blue/ n=20) transects. Background colors indicate broad oceanographic regions separated by latitude (blue =
 298 Temperate, red = Subtropical, yellow = Equatorial upwelling regions). Grey spaces between regions represent the
 299 difference in boundaries between the two transects.

300

301 We observed distinct latitudinal, zonal, and hemispheric C:N:P variability (Fig. 3). First,
 302 we detected peak ratios in the subtropical gyres, troughs in the high latitudes, and intermediate
 303 values at the equator for C:N, C:P, and N:P, matching patterns seen globally (Martiny et al.,
 304 2013b). In the subtropical gyres, averaged C:N values were noticeably elevated (7.0 to 7.6)
 305 compared to the other regions (Temperate: 6.0 to 7.2, EQ: 6.6 to 6.8) (Fig. 3a). C:P followed the
 306 same trend as C:N, with subtropical gyre regions being higher (148 to 208) than the other regions
 307 (Temperate: 122 to 158, EQ: 136 to 161) (Fig. 3b). N:P showed parallel changes to C:P except
 308 the South Atlantic Gyre showed a N:P range encompassing those of all other regions (20.1 to
 309 29.2) (Fig. 3c). Second, a zonal gradient was detected, whereby C:N was higher in the eastern

310 side of the South Atlantic Ocean compared to the western side (Fig. 3D). However, this zonal
 311 gradient was not observed in other regions. C:P also showed an opposite zonal trend with higher
 312 values on the western side, albeit only significantly different in the northern hemisphere (Fig.
 313 3e). N:P showed the highest zonal variation. This ratio was significantly higher on the western
 314 (21.4) compared to the eastern side (17.1) of the South Atlantic Subtropical Gyre (Fig. 3f),
 315 converging at $\sim 10^\circ$ S and again elevated on the western side (29.2) compared to the eastern side
 316 (24.8) of the North Atlantic Subtropical Gyre (Fig. 3f). Again, using the 1° cell centered on this
 317 intersection, we determined C:N, C:P, and N:P had a 5.8%, 12.1%, and 5.9% difference,
 318 respectively, between the two cruises. One sample is the cause of a majority of the error, with its
 319 removal the difference becomes 2.6% for C:N and 1% for the rest. Third, there was also a
 320 hemisphere bias, whereby C:P, and N:P were elevated in the northern hemisphere and C:N
 321 somewhat higher in the southern hemisphere. In summary, we saw clear latitudinal, zonal, and
 322 hemisphere gradients in C:N:P across the Atlantic Ocean.



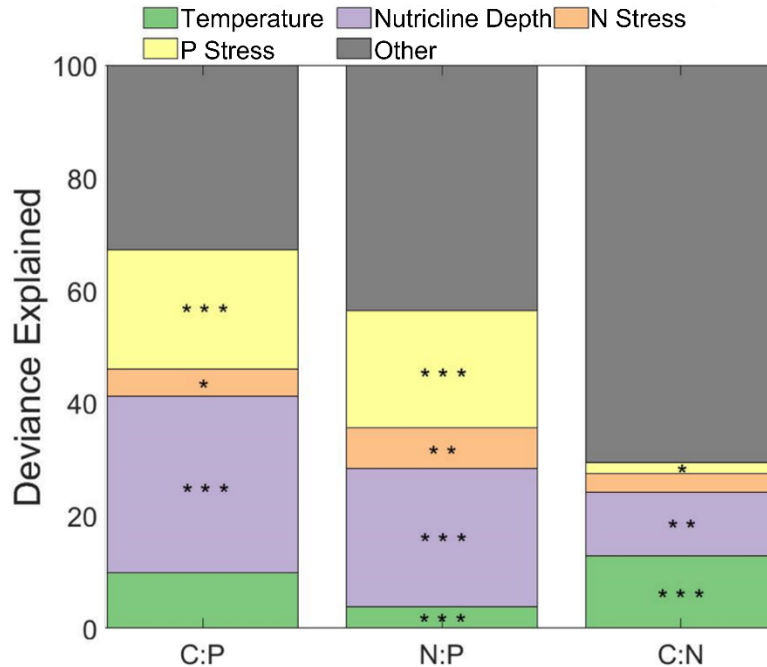
324 **Figure 3.** Latitudinal and regional shifts in POM stoichiometry. (a-c) Averaged observed surface C:N, C:P, and N:P.
 325 The trend lines represent the moving average of samples for AMT28 (red) and C13.5 (blue) transects. Linear
 326 regression line representative of all samples along the transects (black). (d-f) Regional C:N, C:P, and N:P
 327 represented by boxplots, where data were separated by latitude and longitude (E = East, W = West). Significant
 328 zonal (east-west) differences are denoted with * above plot based on Tukey posthoc significant difference test ($p =$
 329 0.05). For all boxplots, a central black bar of the box represents the median value. The whiskers signify the range
 330 (min, max) of values excluding outliers.
 331

332
333
334
335
336
337
338
339
340
341
342
343
344
345
346
347
348
349
350
351
352
353
354
355
356
357
358
359
360
361
362
363
364
365
366
367
368
369
370
371
372

The variability of C:N:P across regions can be partially explained when investigating N* at 200 m for AMT 28. Across the transect, N* has a positive value from 10° N to 50° N, with the remaining regions having a negative value (Fig. S3). As N* decreases from north to south indicating that the environment is becoming more nitrogen stressed. When comparing N* and N:P directly, there is only a weak correlation ($r = 0.48$, $p < 0.001$). Beyond the general increasing value of both N* and N:P from the south to the north, the features of the two plots do not line up directly. Rather it would appear that the peaks in N* more closely align with the troughs in N:P and vice versa.

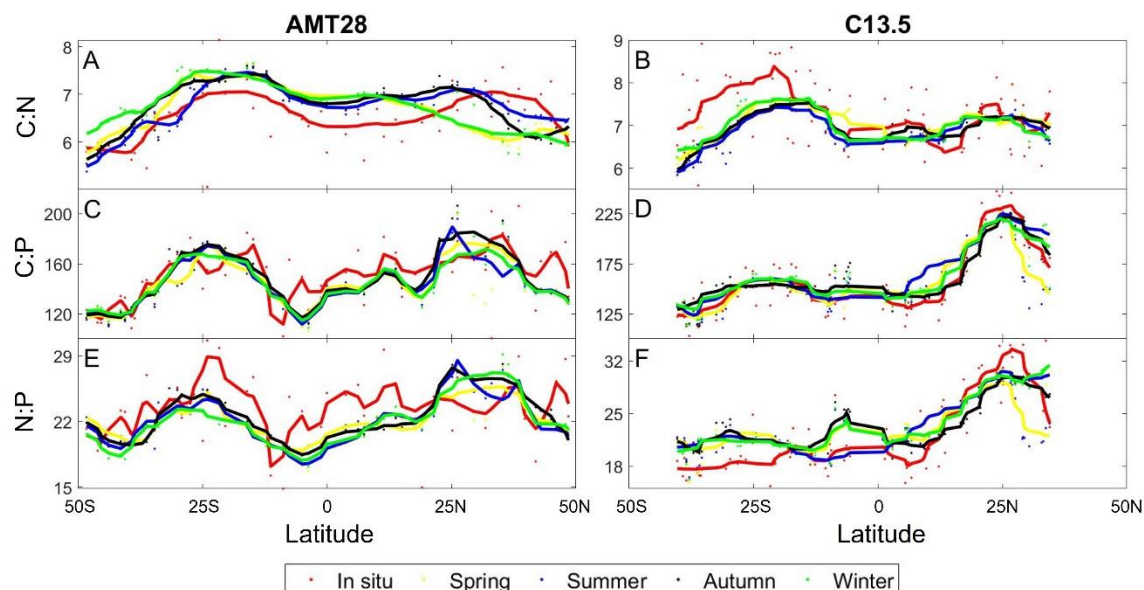
Using flow cytometry cell counts, we were able to determine the concentration and total biomass of separate species of photoautotrophs at each station for AMT 28. From this, *Prochlorococcus* was determined to make up > 93% of the community in the subtropical gyres and equator, and over 50% of the total biomass. 67% of the northern temperate region community consisted of *Prochlorococcus* but only 10% of the biomass, and the South Temperate Atlantic Ocean was the only region without *Prochlorococcus* being the most abundant at 12% of the community and 1% of the biomass (Fig. S4). With the fractional biomass of the six phytoplankton size groups, we used a linear regression model to link to C:P along the transect. The regression model was able to describe the general characteristics of the in situ samples but failed to capture the detailed transitions ($R^2 = 0.23$ $p < 0.05$) (Fig. S5). While only being able to capture the general characteristics of the in situ samples and the dominant biomass of *Prochlorococcus* across the Atlantic, we found that the use of gene specific nutrient stress of *Prochlorococcus* to be an acceptable driver of the variability of C:N:P within GAM.

The influence of phytoplankton composition, temperature, nutricline depth, and metagenomically assessed nitrogen and phosphorus stress (gene index) were tested as drivers of stoichiometry using a general additive model (GAM) (Fig. 4). Using GAM, we determined temperature and the nutrient gene indices captured 67% and 56% of the total deviance for C:P and N:P, respectively. For C:P, nutricline depth and phosphorus gene index accounted for 52.5% of the total (31.3% and 21.2%, respectively). For N:P, nutricline depth and phosphorus gene index accounted for 45% of the total (24.6% and 20.7%, respectively). We could only explain 30% of the total deviance for C:N, with the temperature being the most significant contributors (13% and 11%, $p < 0.001$ and $p < 0.01$ respectively). For C:N:P, nutricline depth was the dominant contributor to the latitudinal variability for two of the three ratios, being the second most dominant in the third, when investigating the entire basin (Fig. 4). When dividing the Atlantic Ocean into eastern and western boundaries, the four drivers tested were able to explain the variability of C:P and N:P more accurately in the western side (81% and 63% respectively) and C:P in the eastern side (38%) (Fig. S7 and S8, Table S2). From this division the dominant drivers remained nutricline depth and temperature for C:P and N:P, and became the dominant driver of C:N. While the drivers for C:N individually have a maximum of 7% difference between each other on either side of the Atlantic Ocean, regional focus is able to interpret changes in drivers that an ocean wide analysis would determine to be different.



373 **Figure 4.** Influence of environmental factors on stoichiometry. Stars indicate the significance of smooth terms used
 374 for Generalized Additive Models (GAM). *** = $p < 0.001$, ** = $p < 0.01$, * = $p < 0.05$. Green represents the
 375 influence of temperature, purple represents the influence of nutricline depth, orange represents the nitrogen stress,
 376 yellow represents the phosphorus stress, and grey represents the remaining factors of influence on the variability of
 377 C:N:P. N and P stress are reflective of the nutrient gene index, which is quantified by calculating the frequency of
 378 the nutrient acquisition genes within *Prochlorococcus* single-copy core genes. The frequency is attributed to the
 379 genetic adaptation for overcoming nutrient stress type and severity.
 380

381
 382 A zonal gradient in nutricline depth and metagenomically assessed nitrogen and
 383 phosphorus stress matched C:N:P shifts (Fig. 3d–f). Nutricline depth was significantly deeper (p
 384 < 0.05) in the western part of subtropical gyres in both hemispheres (Fig. S2). Furthermore, there
 385 was a westward shift from nitrogen towards phosphorus stress (Fig. S6). This zonal shift in
 386 nutrient availability corresponds to a similar increase in C:P from 174 to 207 and N:P from 24.8
 387 to 29.2 towards the western side of the oligotrophic gyres (Fig. 3e, f). In parallel, C:N showed
 388 the opposite trend declining from 7.6 on the eastern to 7.0 on the western side, matching a shift
 389 from nitrogen to phosphorus stress (Fig. 3D). GAM analyses conducted separately for western
 390 and eastern basins corroborated these observations highlighting that the relative importance of
 391 shifting nutrient stress (Fig. S7–9). In summary, zonal variability in nutrient stress, described by
 392 a westward deepening nutricline and increased phosphorus gene index, may regulate a zonal
 393 change in C:N:P.
 394



395
 396 **Figure 5.** Predicted seasonal variability of stoichiometry across the Atlantic Ocean. Observed compared to predicted
 397 seasonal C:N for AMT28 (A) and C13.5 (B). Observed compared to predicted seasonal C:P for AMT28 (C) and
 398 C13.5 (D). Observed compared to predicted seasonal N:P for AMT28 (E) and C13.5 (F). Dots are discrete samples
 399 and the lines are moving averages over ten samples. AMT28 occurred during the fall 2018 and C13.5 during the
 400 spring 2020. In situ samples are red, predicted Spring is yellow, predicted Summer is blue, predicted Autumn is
 401 black, and predicted Winter is green.

402
 403 We assessed the potential impact of seasonal environmental changes for C:N:P across the
 404 Atlantic Ocean. Seasonal environmental changes were characterized as shifts in nutricline depth
 405 and temperature, while assuming a stable biogeography of nitrogen vs. phosphorus stress (Fig.
 406 5). This assumption is the result of only having gene stress information from the season samples
 407 were collected in. As a control, we saw a significant correlation between the observed and
 408 predicted C:N:P for the season matching the cruise occurrence (Table S3). However, the
 409 statistical model did not predict high C:N in the eastern South Atlantic Ocean and overestimated
 410 N:P in the equatorial and western South Atlantic Ocean. C:N:P ratios were predicted to be
 411 mostly stable across seasons. Although we detected shifts in C:N near the north sub-tropical
 412 convergence zone (~18° C) reflecting an expansion and contraction of oligotrophic conditions
 413 (Fig. 5a). The introduction of more dynamic biogeography of nutrient stress will be necessary to
 414 predict a more accurate seasonal variability of C:N:P across the Atlantic Ocean. However, from
 415 data available our statistical model predicted a mostly stable, seasonal C:N:P across the Atlantic
 416 Ocean.

417 418 **4. Discussion**

419
 420 There was clear latitudinal variability in POM concentrations and stoichiometry across the
 421 Atlantic Ocean. We detected a high POM concentration and low C:N:P at higher latitudes, low
 422 POM concentrations and high ratios in the subtropical gyres, and intermediate values near the
 423 equator. This meridional gradient in POM concentrations and ratios corresponded to parallel
 424 changes in nutricline depth and thus likely linked to the overall nutrient supply. Similar gradients
 425 in concentrations and ratios have been detected in the Indian Ocean (Garcia et al., 2018), the
 426 Pacific Ocean (Lee et al., 2021), and in a global synthesis (Martiny et al., 2013b). Thus, our

427 observations add further support to systematic biome shifts in C:N:P across major ocean basins.
428 Despite having similar gradients, the North Atlantic Ocean appears to be relatively unique with
429 higher C:P and N:P ratios in the northern hemisphere compared to the south. Both the North
430 Atlantic and the Indian Ocean's Bay of Bengal have comparable aerolian iron inputs, however,
431 North Atlantic Ocean has an increase in N₂-fixation, which increases the N:P nutrient supply
432 ratio, leading to widespread phosphorus stress (Capone, 2014; Schlosser et al., 2014; Ussher et
433 al., 2013). The Bay of Bengal does not have significant N₂-fixation nor a significant change in
434 C:P or N:P ratios (Garcia et al., 2018; Löscher et al., 2020). This lack of N₂-fixation is possibly
435 the result of stress from another micronutrient for N₂-fixers.

436 Focusing on the influence of P stress, there is an increase in phytoplankton elemental C:P
437 and, to a lesser extent, N:P throughout much of the North Atlantic Ocean. POP has a minimum
438 concentration in the western North Atlantic Ocean (Fig. S1), suggesting that the parallel changes
439 in N:P and C:P are caused by lower POP concentrations. Iron inputs decrease across the North
440 Atlantic Ocean from east to west, with a majority of the POP concentrations following the same
441 trend (Mahowald et al., 2005). While there is an increase in POP concentrations for C13.5, part
442 of this is attributed to coastal upwelling. Had C13.5 continued North it is possible that the POP
443 concentrations observed in the lower half of the North Atlantic gyre would have continued.
444 Proposed explanations of this zonal difference results from a combination of vertical iron supply
445 and lateral circulation across the Atlantic Ocean (Martiny et al., 2019). In the South Atlantic
446 Ocean, aeolian iron inputs are significantly lower, as most dust is washed out at the Intertropical
447 Convergence Zone (Capone, 2014). N₂-fixation is hence suppressed (Wang et al., 2019),
448 allowing most of the southern hemisphere to display elevated N stress. This rise in nitrogen
449 stress likely causes the depressed PON concentrations (Fig. S1) and elevated C:N but depressed
450 N:P in much of the South Atlantic Ocean. Thus, the hemisphere deviation in C:N:P is
451 hypothesized to be driven by a causal link between iron inputs, N₂-fixation, and shifts between
452 the nitrogen and phosphorus gene index (Martiny et al., 2019).

453 An additional zonal gradient in C:N:P may be linked to the westward deepening of the
454 nutricline and a parallel shift from primarily nitrogen stress towards an increase in phosphorus
455 stress. Phosphorus stress is detected throughout the central North Atlantic Ocean based on both
456 the gene index and N* (Ustick et al., 2021), however both C:P and N:P are significantly higher
457 on the western side. Using the nutricline depth as proxy of nutrient supply, the nutrient supply
458 appeared greater on the eastern side, in addition, aeolian nutrient inputs could relieve nutrient
459 stress towards the east, suppressing C:P and N:P ratios (Kremling and Streu, 1993; Mills et al.,
460 2004; Garcia et al., 2018; Neuer et al., 2004). The South Atlantic Ocean also has the east-west
461 variability for C:N:P, C:N having the largest gradient. From the nutrient gene index and N*, the
462 South Atlantic Ocean is predominantly nitrogen stressed. Zonal shifts in C:N:P can be explained
463 by shallower nutricline depth and a higher nitrogen gene index in the eastern part and higher
464 phosphorus gene index in the western part of the South Atlantic Ocean (Ustick et al., 2021;
465 Martiny et al., 2019). Thus, we observe zonal variability in POM concentrations and their
466 stoichiometric ratios, superimposed on the larger meridional and hemisphere gradients.

467 Nitrogen and phosphorus stress are assessed based on genomic changes and adaptation in
468 *Prochlorococcus* populations (Ustick et al., 2021). With *Prochlorococcus* being the most
469 abundant phytoplankton and that it forms most of the phytoplankton biomass in the gyres and
470 equatorial regions, and northern temperate population, it is likely closely linked to the bulk
471 phytoplankton community physiological status (Fig. S4) (Marañón et al., 2000; Zwirgmaier et
472 al., 2007). Additionally, *Prochlorococcus* and *Synechococcus* express nearly identical responses

473 across a transect with regions of different nutrient stress (i.e. when *Prochlorococcus* had a high
474 phosphorus gene index, *Synechococcus* had a high phosphorus gene index as well) (Garcia et al.,
475 2020). Within the South Atlantic Ocean, the use of bioassays and deficiency calculations agree
476 with *Prochlorococcus* gene stress, being primarily nitrogen stressed, yet disagree within the
477 North Atlantic Ocean (Browning and Moore, 2023). While previous bottle experiments of
478 nutrient stress in the North Atlantic Ocean describe it as being dominantly or co-stressed by
479 nitrogen and phosphorus, respectively, the gene index describes the North Atlantic as dominantly
480 phosphorus stressed. This suggests that there is a significant difference between the different
481 assays in determining the nutrient stresses phytoplankton experience. This study focused on
482 factors that had direct influence on C:N:P, we then chose to forgo using co-stressors of nutrients
483 or the use of iron stress. Along with direct influence, these samples match one to one with the
484 POM samples collected on the cruises.

485 It was determined through the use of GAM, that nutricline depth, phosphorus stress, and
486 temperature were the main drivers in the variability of C:N:P. These findings are similar to those
487 of a global synthesis that determined nutricline and gene index were the dominant drivers of
488 C:N:P variability within the tropical and subtropical regions (Tanioka et al., 2022). While their
489 pole-wards assessment determined that temperature was the dominant driver, the samples used
490 in this study fall primarily within tropical/ subtropical bounds (49 of 877 samples are outside of
491 this range). C:P and N:P generally agreed with this global model assessment, but C:N
492 temperature had a smaller influence globally than for the Atlantic Ocean. With the relatively
493 small amount of variance determined for C:N, it is possible that the northern most samples had a
494 major impact on the determination of temperature influence, as seen with Tanioka et al., 2022,
495 in which temperature was determined to be the most significant driver for the variance of C:N.
496 With respect to the other section of the GAM analysis, the factors with a more indirect
497 relationship to C:N:P could have a significant role, especially with C:N (i.e. the influence of iron
498 stress or light availability).

499 The predicted restricted changes in seasonal values of C:N:P were able to fall in the
500 middle to lower range of the observed seasonal averages of those observed at BATS,
501 representing the fall and winter seasons better than spring and summer (Singh et al., 2015). It is
502 worth noting that while the values were able to capture the lower range, the ratios measured
503 during C13.5 closest to BATS, were lower than the measured monthly averages. Since C13.5
504 was unable to take CTD measurements, the nutricline depth from WOA might not accurately
505 represent the actual nutricline depth during the transect, leading to potential changes in the
506 predictive seasonal values. The intersection point of the two transects ($\sim 10^\circ$ S) also indicates
507 minimal seasonal influence as the POM and stoichiometric values despite collection occurring in
508 opposite seasons. Using the values predicted by GAM for the same parameters, there was less
509 than a 2% difference in C:N:P between fall and spring indicating that some of the assumptions
510 made with the predictors weakened the sensitivity of the model. Without this sensitivity, the
511 predictive model suggests that the observed biogeography of C:N:P is stable in most of the
512 central Atlantic Ocean. In summary, we detect clear meridional, hemisphere, and zonal
513 gradients in elemental stoichiometry that corresponds to changes in nutrient supply and stress
514 type, but additional factors may also provide a significant influence on regional shifts in C:N:P
515 across the Atlantic Ocean.

516 Our observations from the Atlantic Ocean have implications for predicting future changes
517 to the ocean carbon cycle. Recent models have suggested that C:N:P variability can ‘buffer’ the
518 effects of stratification and reduced nutrient supply on primary productivity and carbon

519 sequestration (Kwon et al., 2022, Tanioka and Matsumoto, 2017). Such models of C:N:P
520 variability have so far been tied to surface phosphate concentrations (Galbraith and Martiny,
521 2015). However, our observations from the Atlantic Ocean indicate that subtle shifts between
522 nitrogen and phosphorus stress can have additional impacts on the elemental stoichiometry. N₂-
523 fixation in the North Atlantic Ocean is likely responsible for part of the shift in nutrient stress
524 type. The hemispheric variability of nutrient stress suggests an additional role of iron supply in
525 regulating C:N:P. Thus, climate change may alter future patterns of C:N:P as the perturbation of
526 air-sea dynamics can modulate the strengths of boundary currents, the slope of a westward
527 nutricline (Kelly et al., 2010), or the aeolian deposition of iron (Krishnamurthy et al., 2010).
528 Such shifts in C:N:P could, in turn, have large impacts on global nitrogen fixation, primary
529 production, or carbon sequestration.

530

531 **Conflict of interest**

532 The authors declare no conflicts of interest relevant to this study.

533

534 **Acknowledgments**

535 We thank the Global Oceans Ship-Based Hydrographic Investigations Program (GO-SHIP) and
536 the Atlantic Meridional Transect Programme for facilitating this project. We extend a special
537 thanks to Andrew Rees, Glen Tarren, and the crew of the *RSS James Clark* and Leticia Barbero
538 and the crew of the *R/V Roger Revelle*. This research was funded by the National Science
539 Foundation (OCE-1848576 and 1948842 to ACM), NASA (80NSSC21K1654 to ACM), NOAA
540 (101813 Z7554214 to ACM), and Simons Postdoctoral Fellowship in Marine Microbial Ecology
541 (724483 to TT). The PML AMT is funded by the UK Natural Environment Research Council
542 through its National Capability Long-term Single Centre Science Program, Climate Linked
543 Atlantic Sector Science (grant number NE/R015953/1). This study contributes to the
544 international IMBeR project and is AMT contribution number XXX (number pending).

545

546 **Data availability statement**

547 The AMT data set presented here is publicly hosted by the British Oceanographic Data Centre
548 (<https://doi.org/10.5285/b5900384-89f0-3a38-e053-6c86abc0409d>). Hydrographic data from the
549 AMT28 transect are available (<https://cchdo.ucsd.edu/cruise/74JC20180923>). The particulate
550 organic matter data from the C13.5 transect are available here
551 (<https://www.bco-dmo.org/dataset/868908>). Hydrographic data from C13.5 data are available
552 (<https://cchdo.ucsd.edu/cruise/33RO20200321>). Nutricline depth for C13.5 is calculated from
553 gridded annual mean nitrate data from World Ocean Atlas 2018
554 (<https://www.ncei.noaa.gov/data/oceans/woa/WOA18/DATA/>).

555

556 **References**

557 Babiker, I. S., Mohamed, M. A. A., Komaki, K., Ohta, K., and Kato, K.: Temporal Variations in
558 the Dissolved Nutrient Stocks in the Surface Water of the Western North Atlantic Ocean, *Journal*
559 *of Oceanography*, 60, 553–562, <https://doi.org/10.1023/B:JOCE.0000038348.66907.db>, 2004.

560 Browning, T. J. and Moore, C. M.: Global analysis of ocean phytoplankton nutrient limitation
561 reveals high prevalence of co-limitation, *Nat Commun*, 14, 5014,
562 <https://doi.org/10.1038/s41467-023-40774-0>, 2023.

563 Capone, D. G.: An iron curtain in the Atlantic Ocean forms a biogeochemical divide,
564 Proceedings of the National Academy of Sciences, 111, 1231–1232,
565 <https://doi.org/10.1073/pnas.1322568111>, 2014.

566 Cavender-Bares, K. K., Karl, D. M., and Chisholm, S. W.: Nutrient gradients in the western
567 North Atlantic Ocean: Relationship to microbial community structure and comparison to patterns
568 in the Pacific Ocean, Deep Sea Research Part I: Oceanographic Research Papers, 48, 2373–2395,
569 [https://doi.org/10.1016/S0967-0637\(01\)00027-9](https://doi.org/10.1016/S0967-0637(01)00027-9), 2001.

570 Cermeño, P., Dutkiewicz, S., Harris, R. P., Follows, M., Schofield, O., and Falkowski, P. G.: The
571 role of nutricline depth in regulating the ocean carbon cycle, Proceedings of the National
572 Academy of Sciences, 105, 20344–20349, <https://doi.org/10.1073/pnas.0811302106>, 2008.

573 Clayton, S., Alexander, H., Graff, J. R., Poulton, N. J., Thompson, L. R., Benway, H., Boss, E.,
574 and Martiny, A.: Bio-GO-SHIP: The Time Is Right to Establish Global Repeat Sections of Ocean
575 Biology, Frontiers in Marine Science, 8, <https://doi.org/10.3389/fmars.2021.767443>, 2022.

576 Cotner, J., Ammerman, J., Peele, E., and Bentzen, E.: Phosphorus-limited bacterioplankton
577 growth in the Sargasso Sea, Aquatic Microbial Ecology, 13, 141–149,
578 <https://doi.org/10.3354/ame013141>, 1997.

579 Ducklow, H. and Dickson, A.: Shipboard sampling procedures, 1994.

580 Galbraith, E. D. and Martiny, A. C.: A simple nutrient-dependence mechanism for predicting the
581 stoichiometry of marine ecosystems, Proceedings of the National Academy of Sciences, 112,
582 8199–8204, <https://doi.org/10.1073/pnas.1423917112>, 2015.

583 Garcia, C. A., Baer, S. E., Garcia, N. S., Rauschenberg, S., Twining, B. S., Lomas, M. W., and
584 Martiny, A. C.: Nutrient supply controls particulate elemental concentrations and ratios in the
585 low latitude eastern Indian Ocean, Nature Communications, 9, 4868,
586 <https://doi.org/10.1038/s41467-018-06892-w>, 2018.

587 Garcia, C. A., Hagstrom, G. I., Larkin, A. A., Ustick, L. J., Levin, S. A., Lomas, M. W., and
588 Martiny, A. C.: Linking regional shifts in microbial genome adaptation with surface ocean
589 biogeochemistry, Philosophical Transactions of the Royal Society B: Biological Sciences, 375,
590 20190254, <https://doi.org/10.1098/rstb.2019.0254>, 2020.

591 Isles, P. D. F.: The misuse of ratios in ecological stoichiometry, Ecology, 0, 1–7,
592 <https://doi.org/10.1002/ecy.3153>, 2020.

593 Kelly, K. A., Small, R. J., Samelson, R. M., Qiu, B., Joyce, T. M., Kwon, Y. O., and Cronin, M.
594 F.: Western boundary currents and frontal air-sea interaction: Gulf stream and Kuroshio
595 Extension, Journal of Climate, 23, 5644–5667, <https://doi.org/10.1175/2010JCLI3346.1>, 2010.

596 Kremling, K. and Streu, P.: Saharan dust influenced trace element fluxes in deep North Atlantic
597 subtropical waters, Deep Sea Research Part I: Oceanographic Research Papers, 40, 1155–1168,
598 [https://doi.org/10.1016/0967-0637\(93\)90131-L](https://doi.org/10.1016/0967-0637(93)90131-L), 1993.

599 Krishnamurthy, A., Moore, J. K., Mahowald, N., Luo, C., and Zender, C. S.: Impacts of
600 atmospheric nutrient inputs on marine biogeochemistry, *Journal of Geophysical Research*, 115,
601 G01006, <https://doi.org/10.1029/2009JG001115>, 2010.

602 Lee, J. A., Garcia, C. A., Larkin, A. A., Carter, B. R., and Martiny, A. C.: Linking a Latitudinal
603 Gradient in Ocean Hydrography and Elemental Stoichiometry in the Eastern Pacific Ocean,
604 *Global Biogeochemical Cycles*, 35, <https://doi.org/10.1029/2020GB006622>, 2021.

605 Lomas, M. W., Burke, A. L., Lomas, D. A., Bell, D. W., Shen, C., Dyhrman, S. T., and
606 Ammerman, J. W.: Sargasso Sea phosphorus biogeochemistry: An important role for dissolved
607 organic phosphorus (DOP), *Biogeosciences*, 7, 695–710, <https://doi.org/10.5194/bg-7-695-2010>,
608 2010.

609 Lomas, M. W., Bates, N. R., Johnson, R. J., Steinberg, D. K., and Tanioka, T.: Adaptive carbon
610 export response to warming in the Sargasso Sea, *Nature Communications*, 13, 1211,
611 <https://doi.org/10.1038/s41467-022-28842-3>, 2022.

612 Löscher, C. R., Mohr, W., Bange, H. W., and Canfield, D. E.: No nitrogen fixation in the Bay of
613 Bengal?, *Biogeosciences*, 17, 851–864, <https://doi.org/10.5194/bg-17-851-2020>, 2020.

614 Mahowald, N. M., Baker, A. R., Bergametti, G., Brooks, N., Duce, R. A., Jickells, T. D.,
615 Kubilay, N., Prospero, J. M., and Tegen, I.: Atmospheric global dust cycle and iron inputs to the
616 ocean, *Global Biogeochemical Cycles*, 19, <https://doi.org/10.1029/2004GB002402>, 2005.

617 Marañón, E., Holligan, P. M., Varela, M., Mouriño, B., and Bale, A. J.: Basin-scale variability of
618 phytoplankton biomass, production and growth in the Atlantic Ocean, *Deep Sea Research Part I:
619 Oceanographic Research Papers*, 47, 825–857, [https://doi.org/10.1016/S0967-0637\(99\)00087-4](https://doi.org/10.1016/S0967-0637(99)00087-4),
620 2000.

621 Martiny, A. C., Vrugt, J. A., Primeau, F. W., and Lomas, M. W.: Regional variation in the
622 particulate organic carbon to nitrogen ratio in the surface ocean, *Global Biogeochemical Cycles*,
623 27, 723–731, <https://doi.org/10.1002/gbc.20061>, 2013a.

624 Martiny, A. C., Pham, C. T. A., Primeau, F. W., Vrugt, J. A., Moore, J. K., Levin, S. A., and
625 Lomas, M. W.: Strong latitudinal patterns in the elemental ratios of marine plankton and organic
626 matter, *Nature Geoscience*, 6, 279–283, <https://doi.org/10.1038/ngeo1757>, 2013b.

627 Martiny, A. C., Lomas, M. W., Fu, W., Boyd, P. W., Chen, Y. L., Cutter, G. A., Ellwood, M. J.,
628 Furuya, K., Hashihama, F., Kanda, J., Karl, D. M., Kodama, T., Li, Q. P., Ma, J., Moutin, T.,
629 Woodward, E. M. S., and Moore, J. K.: Biogeochemical controls of surface ocean phosphate,
630 *Science Advances*, 5, eaax0341, <https://doi.org/10.1126/sciadv.aax0341>, 2019.

631 Mather, R. L., Reynolds, S. E., Wolff, G. A., Williams, R. G., Torres-Valdes, S., Woodward, E.
632 M. S., Landolfi, A., Pan, X., Sanders, R., and Achterberg, E. P.: Phosphorus cycling in the North
633 and South Atlantic Ocean subtropical gyres, *Nature Geoscience*, 1, 439–443,
634 <https://doi.org/10.1038/ngeo232>, 2008.

635 Michaels, A. F. and Knap, A. H.: Overview of the U.S. JGOFS Bermuda Atlantic Time-series
636 Study and the Hydrostation S program, *Deep Sea Research Part II: Topical Studies in*
637 *Oceanography*, 43, 157–198, [https://doi.org/10.1016/0967-0645\(96\)00004-5](https://doi.org/10.1016/0967-0645(96)00004-5), 1996.

638 Michaels, A. F., Knap, A. H., Dow, R. L., Gundersen, K., Johnson, R. J., Sorensen, J., Close, A.,
639 Knauer, G. A., Lohrenz, S. E., Asper, V. A., Tuel, M., and Bidigare, R.: Seasonal patterns of
640 ocean biogeochemistry at the U.S. JGOFS Bermuda Atlantic time-series study site, *Deep Sea*
641 *Research Part I: Oceanographic Research Papers*, 41, 1013–1038, [https://doi.org/10.1016/0967-](https://doi.org/10.1016/0967-0637(94)90016-7)
642 [0637\(94\)90016-7](https://doi.org/10.1016/0967-0637(94)90016-7), 1994.

643 Mills, M. M., Ridame, C., Davey, M., La Roche, J., and Geider, R. J.: Iron and phosphorus co-
644 limit nitrogen fixation in the eastern tropical North Atlantic, *Nature*, 429, 292–294,
645 <https://doi.org/10.1038/nature02550>, 2004.

646 Moreno, A. R., Larkin, A. A., Lee, J. A., Gerace, S. D., Tarran, G. A., and Martiny, A. C.:
647 Regulation of the Respiration Quotient Across Ocean Basins, *AGU Advances*, 3,
648 [e2022AV000679](https://doi.org/10.1029/2022AV000679), <https://doi.org/10.1029/2022AV000679>, 2022.

649 Neuer, S., Torres-Padrón, M. E., Gelado-Caballero, M. D., Rueda, M. J., Hernández-Brito, J.,
650 Davenport, R., and Wefer, G.: Dust deposition pulses to the eastern subtropical North Atlantic
651 gyre: Does ocean’s biogeochemistry respond?, *Global Biogeochemical Cycles*, 18, n/a-n/a,
652 <https://doi.org/10.1029/2004GB002228>, 2004.

653 R Core Team: *R: A Language and Environment for Statistical Computing*, 2021.

654 Schlitzer, R.: *Ocean Data View*, 2019.

655 Schlosser, C., Klar, J. K., Wake, B. D., Snow, J. T., Honey, D. J., Woodward, E. M. S., Lohan,
656 M. C., Achterberg, E. P., and Mark Moore, C.: Seasonal ITCZ migration dynamically controls
657 the location of the (sub)tropical Atlantic biogeochemical divide, *Proceedings of the National*
658 *Academy of Sciences of the United States of America*, 111, 1438–1442,
659 <https://doi.org/10.1073/pnas.1318670111>, 2014.

660 Singh, A., Baer, S. E., Riebesell, U., Martiny, A. C., and Lomas, M. W.: C : N : P stoichiometry
661 at the Bermuda Atlantic Time-series Study station in the North Atlantic Ocean, *Biogeosciences*,
662 12, 6389–6403, <https://doi.org/10.5194/bg-12-6389-2015>, 2015.

663 Steinberg, D. K., Carlson, C. A., Bates, N. R., Johnson, R. J., Michaels, A. F., and Knap, A. H.:
664 Overview of the US JGOFS Bermuda Atlantic Time-series Study (BATS): a decade-scale look at
665 ocean biology and biogeochemistry, *Deep Sea Research Part II: Topical Studies in*
666 *Oceanography*, 48, 1405–1447, [https://doi.org/10.1016/S0967-0645\(00\)00148-X](https://doi.org/10.1016/S0967-0645(00)00148-X), 2001.

667 Swift, J.: CTD data from Cruise 74JC20180923, <https://doi.org/10.7942/C2D08M>, 2019.

668 Tanioka, T. and Matsumoto, K.: Buffering of Ocean Export Production by Flexible Elemental
669 Stoichiometry of Particulate Organic Matter, *Global Biogeochemical Cycles*, 31, 1528–1542,
670 <https://doi.org/10.1002/2017GB005670>, 2017.

671 Tanioka, T. and Matsumoto, K.: A meta-analysis on environmental drivers of marine
672 phytoplankton, *Biogeosciences*, 17, 2939–2954, <https://doi.org/10.5194/bg-17-2939-2020>, 2020.

673 Tanioka, T., Garcia, C. A., Larkin, A. A., Garcia, N. S., Fagan, A. J., and Martiny, A. C.: Global
674 patterns and predictors of C:N:P in marine ecosystems, *Commun Earth Environ*, 3, 1–9,
675 <https://doi.org/10.1038/s43247-022-00603-6>, 2022.

676 Ussher, S. J., Achterberg, E. P., Powell, C., Baker, A. R., Jickells, T. D., Torres, R., and
677 Worsfold, P. J.: Impact of atmospheric deposition on the contrasting iron biogeochemistry of the
678 North and South Atlantic Ocean, *Global Biogeochemical Cycles*, 27, 1096–1107,
679 <https://doi.org/10.1002/gbc.20056>, 2013.

680 Ustick, L. J., Larkin, A. A., Garcia, C. A., Garcia, N. S., Brock, M. L., Lee, J. A., Wiseman, N.
681 A., Moore, J. K., and Martiny, A. C.: Metagenomic analysis reveals global-scale patterns of
682 ocean nutrient limitation, *Science*, 372, 287–291, <https://doi.org/10.1126/science.abe6301>, 2021.

683 Utermöhl, H.: Zur Vervollkommnung der quantitativen Phytoplankton-Methodik, *Internationale*
684 *Vereinigung für Theoretische und Angewandte Limnologie: Mitteilungen*, 9, 1–38,
685 <https://doi.org/10.1080/05384680.1958.11904091>, 1958.

686 Wang, W.-L., Moore, J. K., Martiny, A. C., and Primeau, F. W.: Convergent estimates of marine
687 nitrogen fixation, *Nature*, 566, 205–211, <https://doi.org/10.1038/s41586-019-0911-2>, 2019.

688 Weber, T. S. and Deutsch, C.: Ocean nutrient ratios governed by plankton biogeography, *Nature*,
689 467, 550–554, <https://doi.org/10.1038/nature09403>, 2010.

690 Wood, S. N.: *Generalized Additive Models*, Chapman and Hall/CRC,
691 <https://doi.org/10.1201/9781315370279>, 2017.

692 Yvon-Durocher, G., Dossena, M., Trimmer, M., Woodward, G., and Allen, A. P.: Temperature
693 and the biogeography of algal stoichiometry, *Global Ecology and Biogeography*, 24, 562–570,
694 <https://doi.org/10.1111/geb.12280>, 2015.

695 Zwirgmaier, K., Heywood, J. L., Chamberlain, K., Woodward, E. M. S., Zubkov, M. V., and
696 Scanlan, D. J.: Basin-scale distribution patterns of picocyanobacterial lineages in the Atlantic
697 Ocean, *Environmental Microbiology*, 9, 1278–1290, [https://doi.org/10.1111/j.1462-](https://doi.org/10.1111/j.1462-2920.2007.01246.x)
698 [2920.2007.01246.x](https://doi.org/10.1111/j.1462-2920.2007.01246.x), 2007.

699